Available online at www.sciencedirect.com
SCIENCE DIRECT
Catalysis Today 107–108 (2005) 606–611
CATALYSIS TODAY
www.elsevier.com/locate/cattod

Sol–gel titanium oxides sensitized by nanometric carbon blacks: Comparison with the optoelectronic and photocatalytic properties of physical mixtures

M.E. Rincón *, M.E. Trujillo-Camacho, A.K. Cuentas-Gallegos

Centro de Investigación en Energía-UNAM, Apartado Postal 34, Temixco 62580, MOR, Mexico

Available online 22 August 2005

Abstract

The preparation, optical properties and photocatalytic activity of TiO_2/carbon blacks composites as a function of TiO_2 crystallite size are reported. Carbon-doped TiO_2, evidenced by a well defined visible absorption at 1.3 eV, is grown in situ by sol–gel techniques, using $TiCl_4$ as the oxide precursor and ammonia as the basic catalyst. For the physical mixtures of carbon blacks with titanium oxides, at similar composition and thermal treatment, sensitization is not observed regardless of the oxide crystallite size. The core-shell microstructure of the sol–gel materials (i.e. defects at the interface) and/or the presence of a nitrogen base seem relevant for carbon-doping. In general, sol–gel composites outperformed the physical mixtures in the photocatalytic degradation of methyl violet dyes, and the data suggest that this enhancement is mainly due to the role of carbon during carrier photogeneration and transport and not just to the superior surface area of the sol–gel catalysts.

Keywords: Sensitization; Sol–gel; Titanium oxide; Carbon black; Optoelectronic properties

1. Introduction

Titanium dioxide has been broadly explored as an inexpensive photocatalyst that uses sunlight as energy source to degrade environmental pollutants [1]. This photocatalytic degradation is carried out by several steps, being one of them the absorption of photons by TiO_2 which produces the hole–electron pairs required for photodegradation. In this sense, numerous research works have been carried out by chemically modifying TiO_2 to reduce its band-gap energy so that absorbs sunlight over a broader range of wavelengths [2–5]. Reports on the sensitization of titanium oxide by inorganic particles [6–10], narrow band inorganic semiconductors [4,5,11,12], and by nitrogen doping [2,3,13,14], are abundant in the literature and the results so far have been mixed.

Another important aspect in photocatalyst performance is the fast transfer of photogenerated carriers at the semiconductor surface. Large surface area semiconductors, usually in the nano-size range, have the advantage of a great interaction surface, which could lead to fast charge transfer kinetics [15,16]. Still, in these materials the energy band structure is not completely developed, and the orbitals on a given band are quantized. This quantization phenomenon gives way to numerous anomalies on the particles properties, including its optical absorption, in which the decrease in particle size results in the onset of absorption shifted to shorter wavelengths (blue shift) [17]. Thus, the production of nanoparticles renders materials with superior surface area and large band-gap energy. However, the presence of a second element seems necessary to aid the charge generation (doping) and the charge separation (rectification) events, without sacrificing surface area.

Carbon particles have been used in the elaboration of composite photocatalysts with several purposes. For example, as adsorbent agents that concentrates organic contaminants on the semiconductor surface [18–21], as dispersants that avoids photocatalyst agglomeration and increases the effective surface area [19,20,22], and as doping

* Corresponding author. Tel.: +52 555 6229748; fax: +52 777 3250018.
E-mail address: merg@cie.unam.mx (M.E. Rincón).

0920-5861/$ – see front matter © 2005 Elsevier B.V. All rights reserved.
doi:10.1016/j.cattod.2005.07.026

agents that shift the optical response from UV to the visible range [3,23]. In a recent report [24], carbon-sensitized TiO_2 catalysts were prepared by hydrolyzing $TiCl_4$ with tetrabutylammonium hydroxide, followed by calcining the solid up to the complete removal of the nitrogen, leaving a carbon-doped TiO_2. This method was an improvement over the previously reported method to make carbon-doped TiO_2 by pyrolyzing titanium foil in a natural gas flame [25].

In this work we study the effect of nanometric carbon black on the optical properties of TiO_2 materials as a function of TiO_2 crystallite size, and also the chemical or physical elaboration of the composites. Surprisingly, the sol–gel route, usually associated to the production of nanoparticles with superior surface area but also larger band-gap, render the sensitized-TiO_2 materials. The correlation between the optical properties and the photocatalytic degradation of methyl violet-8 (MV-8) is also discussed.

2. Experimental

2.1. Sol–gel synthesis of TiO_2/carbon black photocatalysts

Nanometric TiO_2 was prepared by the sol–gel technique at low temperature (0 °C). Briefly, 2.8 mL $TiCl_4$ (Merck-Schuchardt, A.C.S. reagent) were added (drop by drop) to 100 mL 1 M HCl (HCl 37%, Aldrich A.C.S. reagent) aqueous solution. Immediately after addition, the extremely low pH was adjusted to a value of 3 with concentrated ammonia (HCl 37%, Aldrich A.C.S. reagent). After vigorous stirring for 24 h, 2 g of precipitates were obtained by *sol* neutralization with concentrated ammonia. These solids were washed abundantly with distilled water and dehydrated at 100 °C. For the case of TiO_2 with 10 wt.% carbon blacks (CB), a similar procedure was followed with the proper amount of CB dispersed as an ink prior to the addition of $TiCl_4$. The ink contained small amounts of propylenglycol and triton X-100. These carbon blacks were supplied by Columbian Chemicals Co. and correspond to turbostratic carbons with 123 m^2/g surface area and 20 nm particle size. Thermal treatments were carried out at 300 °C during 1 h in order to eliminate most of the water and organic materials. For comparison, commercial TiO_2 (spectrum, grain size = 30 nm) was also mixed with 10 wt.% carbon blacks until complete homogenization. Screen-printed and sintered films on stainless steel and Corning Glass substrates were elaborated. After further annealing at 450 °C for 1 h in air (films w/o CB) and N_2 (films with CB), the thickness of the films was in the range of 7–13 μm. Annealing assures the conversion of oxo-hydroxides into oxides and removes all the organic components of the film leaving only the TiO_2 structure and CB.

2.2. Structural, optical and photocatalytic characterization

The crystallite size and crystalline phases of these materials were determined by X-ray diffraction using a Rigaku Ultima+ Diffractometer with Cu Kα radiation (λ = 1.54 Å). Optical characterization was carried out in a UV–vis–NIR Shimadzu UV-3101 PC spectrophotometer equipped with a reflectance integration sphere.

To explore the photocatalytic activity of the new materials, the degradation of methyl violet (MV-8) by UV light (365 nm) was investigated. Screen-printed films (1 in. × 1 in.) of the various materials were immersed in 7.2×10^{-5} M methyl violet (MV-8) buffered solution kept at room temperature in Vycor crucibles. Equilibrium under dark conditions was allowed during 30 min, followed by illumination with a 6 W lamp (UVL-56) with 1.24 W/m^2 light intensity. Dye degradation was monitored by UV–vis-spectrophotometry studies (UV–vis Shimadzu UV-1601) at λ = 584.8 nm for a period of time from 0 to 15 h.

3. Results and discussion

3.1. Structural and optical properties

The XRD-pattern of TiO_2 powders synthesized by the sol–gel route and annealed at 400–450 °C in N_2 is compared to that of commercial TiO_2 in Fig. 1(a) and (b), respectively. Screen-printed composites films containing 10–20 wt.% CB show similar diffraction patterns, as can be observed in Fig. 2.

The crystallite size of TiO_2 (Table 1) is obtained from the largest peak appearing at $2\theta = 25°$ by using Scherrer's formula $D = 0.9\lambda/\beta \cos\theta$, where λ is the wavelength of the X-ray radiation (λ = 0.15418 nm), θ the diffracting angle, and β the line-width at half-maximum (FWHM) (in radians) [26]. It is important to emphasize that the physical mixtures and the sol–gel composites could differ not only on crystallite size, but also on TiO_2/CB microstructure, since carbon materials become coated by TiO_2 during the sol–gel synthesis forming core-shell geometries [27,28]. Moreover, minor peaks assigned to the rutile phase are observed in sol–gel powders while commercial TiO_2 (anatase) is free of rutile up to 600 °C.

The optical properties of the various films were determined from the diffuse reflectance spectra and the Kubelka–Munk function given by Eq. (2):

$$\frac{\alpha}{s} = \frac{(1-R)^2}{2R} \tag{2}$$

Here α and s are the absorption and dispersion coefficients, respectively, and R the diffuse reflectance. For these materials, the dispersion coefficient is nearly constant in the studied wavelength interval. Comparison

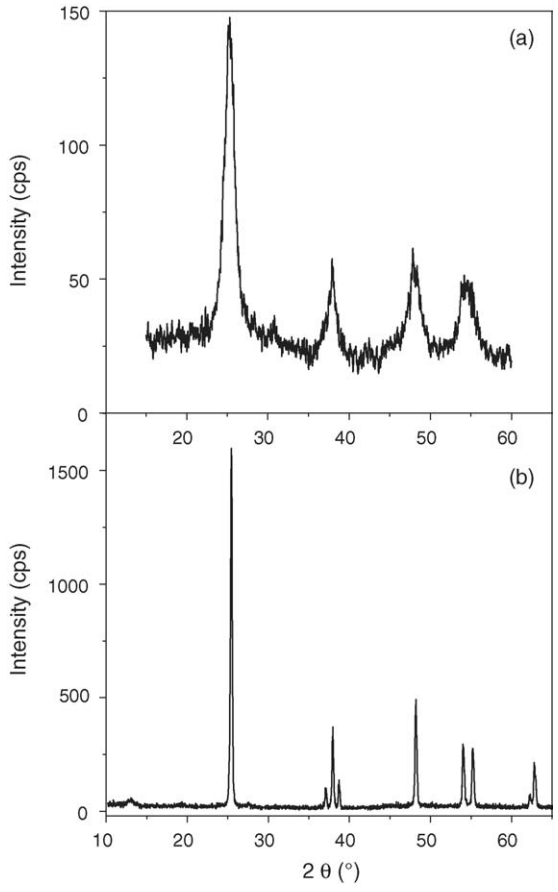

Fig. 1. X-ray powder diffraction patterns of sol–gel TiO_2 precipitates (a) and commercial TiO_2 powders (b) annealed at 400 °C in air during 1 h.

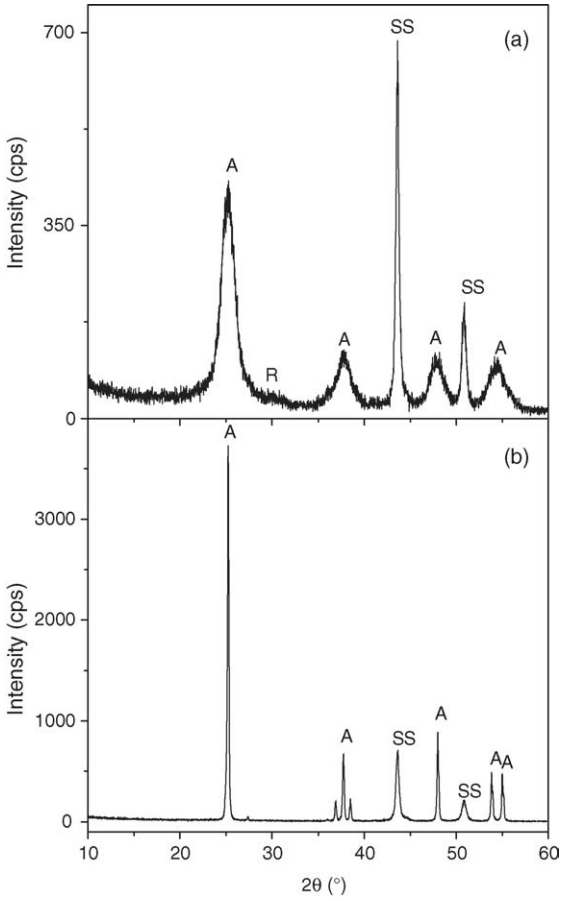

Fig. 2. XRD-patterns of screen-printed films based on sol–gel TiO_2/CB composites (a) and commercial TiO_2/CB mixtures (b). The films were deposited on stainless steel substrates and annealed in N_2 at 400 °C during 1 h. A = anatase; R = rutile; SS = substrate.

between the diffuse reflectance spectra of the commercial and the sol–gel TiO_2 catalysts is given in Fig. 3, while the spectra of the physical mixture and the sol–gel composite with 10 wt.% CB content are shown in Fig. 4. The spectra reveal absorption peaks related to TiO_2 (∼3.1 eV) and carbon black (∼0.8 eV), and a new absorption peak at 1.3 eV in the composite catalyst obtained by the sol–gel route. Assuming the materials to be indirect semiconductors, like TiO_2, their band-gap-energy (E_g) was obtained by means of Eq. (3):

$$\alpha = A(h\nu - E_g)^2 \quad (3)$$

Thus, a plot of the modified Kubelka–Munk function $(\alpha E/s)^{1/2}$ versus the energy of exciting light (E) affords the determination of E_g. Such curves are shown in Figs. 3 and 4 (right axis), while Table 1 lists the crystallite size and band-gap-energy of the various photocatalysts. No increment in band-gap-energy, expected from the smaller crystallite size, is observed for the TiO_2 synthesized by the sol–gel route. The carbon addition causes a 0.10 eV increment in the band-gap energy of TiO_2. This is more notorious for the sol–gel materials, in which a well defined transition near the middle of the TiO_2 band-gap energy (i.e., at 1.3 eV) is the most striking feature. In contrast to these results, band-gap narrowing of 0.05–0.14 eV has been observed for carbon-doped TiO_2 [24], in which the absorption starting at 1.7 eV has been explained by the presence of surface states located close to the valence-band edge.

From our data we can conclude that the method of synthesis determines the optical properties of the composite

Table 1
Crystallite sizes (d) and band-gap energies as a function of the preparation method, annealing temperature and carbon blacks content

Sample	Carbon (%)	Annealing (temperature/time) (°C/h)	Crystallite size[a] (nm)	E_g (eV)
$TiO_{2\ spectrum}$	0	400/1	35	3.12
$TiO_{2\ sol–gel}$	0	400/1	5	3.08
$TiO_{2\ spectrum}$/CB	<10	400/1	30	3.18
$TiO_{2\ sol–gel}$/CB	<10	400/1	9	1.3[b]–18

Crystallite sizes calculated from the XRD-peak at $2\theta = 25°$. Band-gap energies obtained from the Kubelka–Munk function assuming indirect optical transitions.

[a] d (nm) = $0.9\lambda/\beta \cos\theta$, where $\lambda = 0.15406$ nm and β is the peak-width at medium height in radians.

[b] Doping state of carbon black.

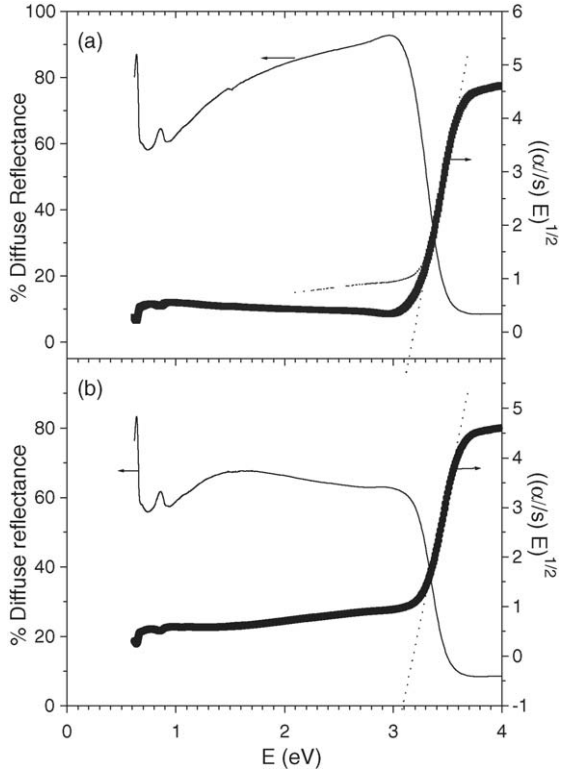

Fig. 3. Diffuse reflectance spectra and indirect optical transition plots for films of: (a) $TiO_{2\ spectra}$; (b) $TiO_{2\ sol–gel}$.

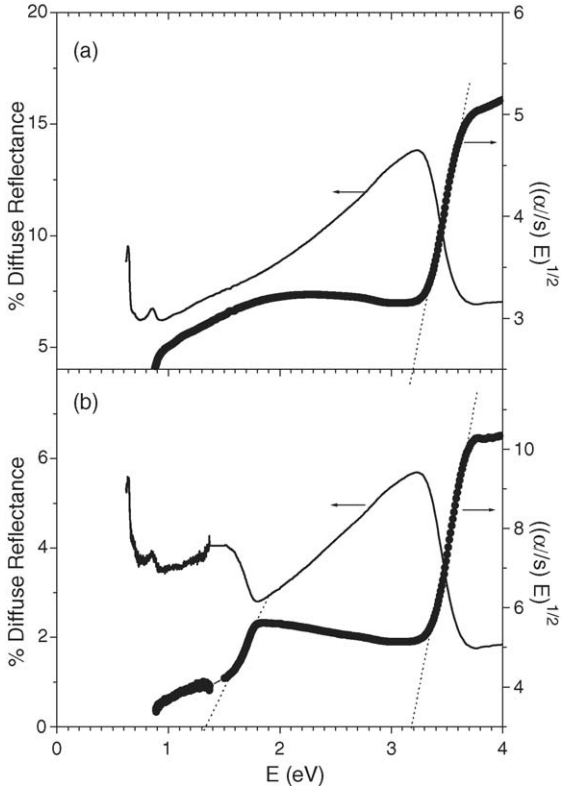

Fig. 4. Diffuse reflectance spectra and indirect optical transition plots for composite films of: (a) $TiO_{2\ spectra}$/CB; (b) $TiO_{2\ sol–gel}$/CB.

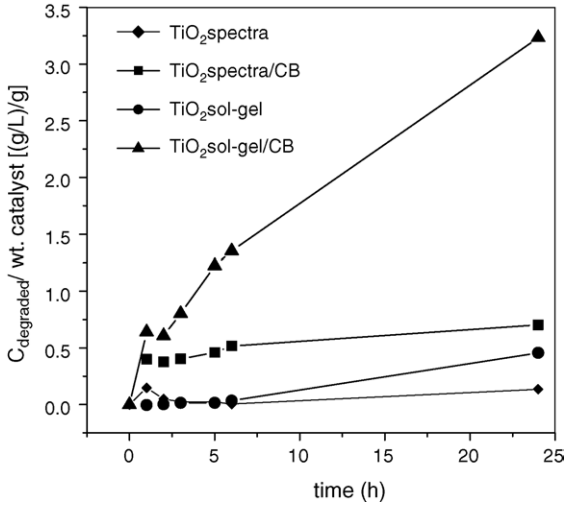

Fig. 5. Amount of MV-8 photodegraded by UV light in the presence of the various screen printed films. Films with equivalent thickness and geometric area.

materials, because as equivalent thermal treatment (400 °C in N_2/1 h) and photocatalyst composition (90 wt.% TiO_2 and 10 wt.% CB) were applied to both the physical mixture and the sol–gel composite, carbon-doping was only observed for the latter. The crystallite size of TiO_2 was also ruled out as the factor causing the differences, by externally mixing 10 wt.% CB with TiO_2 powders obtained from the sol–gel route. However, carbon-doping was not observed in the annealed film of this physical mixture. Therefore, the core-shell microstructure and/or the presence of nitrogen base (i.e., NH_4OH) in the sol–gel bath, as has been discussed in other works [24], seem determinant for the doping mechanism observed. On the contrary, the optical response of the physical mixtures shows the absorption peak of elemental carbon more intense (compare the peaks at 0.8 eV in Fig. 3), almost dominating the dispersive behavior in the low energy zone. In these mixtures, the 20 nm particle size of CB is similar to the 30 nm crystallite size of TiO_2. Data on crystallization, not shown, suggest that CB disrupt TiO_2 grain growth in the physical mixtures, but promotes it in the sol–gel bath by acting as a nucleation seed.

3.2. Photocatalytic activity

To explore the photocatalytic activity of these materials, and to asses the relevance of increasing the surface area, the

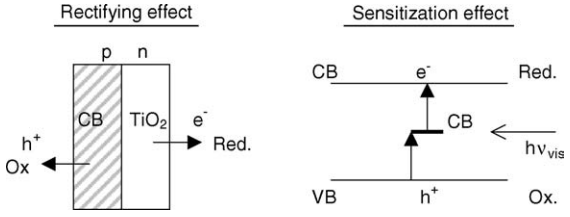

Fig. 6. Schematic representation of the rectifying and doping effects of CB on the electronic properties of TiO_2.

Table 2
Dye-adsorption and photodegradation capacities of (1 in. × 1 in.) films, C_0 (MV-8) = 27 mg/L

Sample	Crystallite size (nm)	Adsorption[a] (mg L^{-1})	Remotion[b] (mg L^{-1})	Initial rate/wt. cat. (mg L^{-1} h^{-1})/g	Photocatalysis (%)
$TiO_{2\ spectrum}$	35	1.2	1.5	125	6
$TiO_{2\ sol-gel}$	5	2.7	8.2	0	21
$TiO_{2\ spectrum}$/CB	30	4.2	5.4	375	32
$TiO_{2\ sol-gel}$/CB	9	4.6	22.6	650	88

[a] Adsorption (A) under dark during 24 h.
[b] Remotion (R) under illumination during 24 h.

degradation of a typical dye (MV-8) was investigated. Fig. 5 illustrates the amount of dye removed per gram of catalyst in the screen-printed films. For the commercial TiO_2 film, dye desorption is observed at the beginning of the irradiation experiment, as evidenced by the minimum in the $C_{degraded}$ versus time curve.

Increasing the photocatalyst surface area does not increase substantially the amount of dye-degraded, as can be seen from the curve of the sol–gel TiO_2 film. The addition of CB, on the other hand, enhances the photodegradation of this dye, particularly in the sol–gel composite film, where the sensitization of TiO_2 plays an important role. Fig. 6 shows the schematics of two mechanisms in which carbon black could aid to the generation and transport of the photogenerated carriers. By creating interband states in the semiconducting oxide, carbon-doping helps to visible light carrier generation. Additionally, the weak p-type conductivity of carbon blacks gives way to local electric fields (i.e., rectification through p–n junctions) that might aid to electron/hole separation and transport.

Although parallel work [29] on the adsorption isotherms of these material indicate a slightly superior adsorption capacity for the nanometric composite photocatalysts, the data listed in Table 2 evidence that pollutant concentration near the semiconductor particle does not account for the differences observed under illumination. Carbon-doping and rectification mechanisms are more appropriate to explain the enhancement on the photocatalytic activity of carbon modified TiO_2 photocatalysts.

4. Conclusion

We studied the optical properties and photocatalytic activity of TiO_2/CB composites as a function of TiO_2 crystallite size, and the chemical or physical preparation of the materials. Regardless of similar composition and thermal treatment, TiO_2-sensitization was only observed for composites prepared by the sol–gel route, where the core-shell microstructure of these materials (i.e. defects at the interface) and/or the presence of a nitrogen base seem relevant for carbon-doping. In general, sol–gel composite materials show a better performance on the photocatalytic degradation of MV-8, and adsorption data suggest that the enhancement is not due to a superior surface area, but to the role of carbon during carrier photogeneration and transport.

References

[1] D.M. Blake, NREL/TP-430-22197, National Renewable Energy Laboratory, Golden Co., 1997–1999.
[2] R. Asahi, T. Morikawa, T. Ohwaki, K. Aoki, Y. Taga, Science 392 (2001) 269.
[3] D. Li, H. Haneda, Photochem. Photobiol. Chem. 160 (2003) 203.
[4] R. Suárez-Parra, I. Hernández-Pérez, S. López-Ayala, M.E. Rincón, M.C. Roldán-Ahumada, Solar Energy Mater. Solar Cells 76 (2003) 189.
[5] M.E. Rincón, O. Gómez-Daza, C. Corripio, A. Orihuela, Thin Solid Films 389 (2001) 91.
[6] E. Traversa, M.L.D. Vona, P. Nunziante, S. Licoccia, T. Sasaki, N. Koshizaki, J. Sol-Gel Sci. Technol. 19 (2000) 733.
[7] J.H. Moon, H. Takagi, Y. Fujishiro, M. Awano, J. Mater. Sci. 36 (2001) 949.
[8] D. Dvoranová, V. Brezová, M. Mazúr, M.A. Malati, Appl. Catal. B: Environ. 37 (2002) 91.
[9] D.H. Kim, H.S. Hong, S.J. Kim, J.S. Song, K.S. Lee, Alloys Compd. 375 (2004) 259.
[10] K. Venkata, S. Rao, B. Lavédrine, P. Boule, Photochem. Photobiol. A: Chem. 154 (2003) 189.
[11] A. Fuerte, M.D. Hernández-Alonso, A.J. Maira, A. Martínez-Arias, M. Fernández-García, J.C. Conesa, J. Soria, G. Munuera, Catalysis 212 (2002) 1.
[12] B. Wang, J. Zhao, X. Wang, B. Bai, G. Sheng, P. Peng, J. Fu, Appl. Catal. B: Environ. 39 (2002) 269.
[13] M. Jansen, H.P. Letschert, Nature 404 (2000) 980.
[14] A. Kasahara, K. Nukumizu, G. Hitoki, T. Takada, J.N. Kondo, M. Hara, H. Kobayashi, K. Domen, Phys. Chem. A 106 (2002) 6750.
[15] K.R. Lee, S.J. Kim, J.S. Song, J.H. Lee, Y.J. Chung, S. Park, Am. Ceram. Soc. 85 (2002) 341.
[16] L. Gao, Q. Zhang, Scripta Mater. 44 (2001) 1195.
[17] S.M. Sze, Physics of Semiconductor Device, John Wiley and Sons, New York, 1981.
[18] J.-M. Herrmann, J. Matos, J. Disdier, Ch. Guillard, J. Laine, S. Malato, J. Blanco, Catal. Today 54 (1999) 255.
[19] N. Takeda, N. Iwata, T. Torimoto, H. Yoneyama, J. Catal. 177 (1998) 240.
[20] T. Torimoto, Y. Okawa, N. Takeda, H. Yoneyama, J. Photochem. Photobiol. A: Chem. 103 (1997) 153.
[21] A. Modestov, V. Glezer, I. Marjasin, O. Lev, Phys. Chem. B 101 (1997) 4623.
[22] J. Araña, J.M. Doña-Rodríguez, E. Tello Rendón, C. Garriga i Cabo, O. González-Díaz, J.A. Herrera-Melián, J. Pérez-Peña, G. Colón, J.A. Navío, Appl. Catal. B: Environ. 44 (2003) 161.
[23] C. Lettmann, K. Hildenbrand, H. Kisch, W. Macyk, W.F. Maier, Appl. Catal. B 32 (2001) 215.

[24] S. Sakthivel, H. Kisch (Eds.), Angew. Chem. 42 (2003) 4908.
[25] S.U.M. Khan, M. Al-Shahry, W.B. Ingler, Science 297 (2002) 2243.
[26] C.S. Barret, T.B. Massalski, Structure of Metals, McGraw-Hill, New York, 1966.
[27] T. Hashishin, J. Murashita, A. Joyaza, Y. Kaneko, Ceram. Soc. Jpn. 106 (1998) 1.
[28] P. Vincent, A. Brioude, C. Journet, S. Rabaste, S.T. Purcell, J. Le Brusq, J.C. Plenet, Non-Cryst. Solids 311 (2002) 130.
[29] M.E. Trujillo-Camacho, A.K. Cuentas-Gallegos, M.E. Rincón, Photocatalysts based on nanostructured and microstructured TiO_2 supported on carbon black: surface characterization by dye adsorption and photodegradation studies.